Expressive riverine fluxes over Amazon floodplain units revealed by high resolution 2D modelling

Alice César Fassoni-Andrade[1,2]*, Rodrigo Cauduro Dias de Paiva[1], Sly Wongchuig[3], Claudio Barbosa[4], Fabien Durand[2,5]

[1] Institute of Hydraulic Research, Federal University of Rio Grande do Sul (UFRGS), Porto Alegre, Brazil.

[2] Institute of Geosciences, University of Brasília (UnB), Campus Universitário Darcy Ribeiro, Brasília, Brazil.

[3] Univ. Grenoble Alpes, IRD, CNRS, Grenoble INP, Institut des Géosciences de l'Environnement (IGE, UMR 5001), 38000, Grenoble, France.

[4] Instrumentation Lab for Aquatic Systems (LabISA), Earth Observation Coordination of National Institute for Space Research (INPE), São José dos Campos, SP, Brazil.

[5] Laboratoire d'Etudes en Géophysique et Océanographie Spatiales (LEGOS), Université Toulouse, IRD, CNRS, CNES, UPS, Toulouse, France.

*Corresponding author: Alice Fassoni-Andrade (alice.fassoni@unb.br, alice.fassoni@gmail.com)

Key Points:

- Improved representation of Amazon River/floodplain hydrodynamics from 2D high resolution model
- Floodplain hydrodynamic complexity with flood extent reaching a plateau during floods and significant flood extent and volume hysteresis
- Expressive inflow/outflow over floodplain units of around 80 km, representing up to 20% of the Amazon River discharge

Abstract

Water fluxes in the Amazon River floodplain affect hydrodynamic and ecological processes from local to global scales. Nevertheless, these fluxes remain poorly understood due to difficult access and limited data. In this study, we characterize the hydrodynamics of eight floodplain units of the central Amazon River (40'000 km^2) using the 2D hydraulic model HEC-RAS. High resolution modeling improved the representation of river and floodplain discharge, water surface elevation (77 cm accuracy) and flood extent (~80% - high water period, ~52% -low water period). We have learned 13 lessons about river and floodplain hydrodynamics from the modeling. The most remarkable lessons are that the floodplain is organized in units of about 80 km with upstream inflow and downstream outflow. These gross flows are much larger than the net flows with values of up to 20% of the Amazon River discharge and a residence time around 6 days during floods (several months during low water period). Water extent does not a have strong interannual

variability during floods as the volume stored in the floodplain, possibly due to topographic constrains. Significant flood extent and volume hysteresis, as well as active flow and storage zones on the floodplain, highlight the complexity of floodplain hydrodynamics. Extreme floods strongly impact the onset and duration of the flood of up to 2 months and, consequently, on the period of high connectivity with the river. These findings are important for understanding carbon and sediment fluxes, and the effects of climate change on water fluxes and riparian communities.

1. Introduction

The Amazon is the largest river system in the world, both in terms of the drainage area and discharge. Their seasonal flood pulse induces a large annual variation in water surface elevation in the floodplain and flooded area. The water level amplitude can reach up to 13 m (Birkett et al., 2002) and the water surface extent of the basin varies between 284'200 km^2 and 633'500 km^2 during the high (April-May) and low water (October-November) periods, respectively (Fleischmann et al., 2022; Hess et al., 2015). Moreover, the bidirectional flows and water residence time in the floodplain are dynamic in space and time, and the patterns of water surface elevation variation are complex (Alsdorf et al., 2007; Cao et al., 2018). The Amazon River flood also has a great influence on regional and global processes, such as sediment transport (Armijos et al., 2020; Dunne et al., 1998), local geomorphology (Fricke et al., 2019; Latrubesse & Franzinelli, 2002), vegetation distribution (Ferreira-Ferreira et al., 2014), seed dispersal (Melack et al., 2009), carbon dioxide (Abril et al., 2014) and methane emissions (Basso et al., 2021), and commercial and subsistence fisheries (Duponchelle et al., 2021). Therefore, understanding the water flow between the Amazon River and floodplain is of great importance to better understand these processes.

Due to the extent of the Amazon River floodplain (about 20 to 50 km wide) and its difficult access, in situ measurements of topography, water level, and water flow are limited. The detailed hydrodynamics of the river-floodplain system and the ecological function of the floodplain are therefore poorly known. Hydrologic and hydrodynamic models have been applied to the Amazon basin to understand large-scale hydrodynamics processes and the role of floodplains (Beighley et al., 2009; Coe et al., 2008; Correa et al., 2017; Getirana et al., 2012; Luo et al., 2017; Paiva et al., 2013; Sorribas et al., 2020; Yamazaki et al., 2011). These studies showed that the water flow exchanged between the river and the floodplain has the same order of magnitude as the river discharge (about 10^4 to 10^5 m^3s^{-1}; Sorribas et al., 2020) and can represent between 3% and 40% of the river discharge depending on the period (Getirana et al., 2012; Richey et al., 1989; Sorribas et al., 2020; Wilson et al., 2007). Water stored in floodplains, which can have a residence time of more than 300 days (Sorribas et al., 2020), plays an important role in delaying and attenuating the river's flood wave (Getirana et al., 2012; Paiva et al., 2013; Yamazaki et al., 2011). Although these models adequately represent river hydraulics (e.g., full Saint-Venant equation, particle-tracking model), they are simplified to represent floodplain hydrodynamics, such as bidirectional flows, which can be better represented with two-dimensional numerical models.

Regional applications of two-dimensional hydraulic models allowed better representation of the floodplain hydrodynamics, such as the study by Wilson et al. (2007), where the water exchange between the Amazon River and the adjacent floodplain over a 240 km-long reach was evaluated. As the drainage process in the floodplain in this model was poorly represented due to

errors in the topographic data (Wilson et al., 2007), Yamazaki et al. (2012) and Baugh et al. (2013) have improved the accuracy of this simulation with correction of topographic errors. Despite the improvement, these studies considered the SRTM3 digital elevation model (DEM) in open water areas, where the lakes are represented by a flat surface. The topography of the extensive central Amazon floodplain is difficult to represent using global elevation models, since it is complex and composed of many interconnected lakes and channels (Trigg et al., 2012) and vegetation types (Hess et al., 2015). In addition, Baugh et al. (2013), Paiva et al. (2013), Yamazaki et al. (2012) and Getirana et al. (2012) point out that topography is the main source of uncertainty in modeling flows in the river-floodplain system, as well as being difficult to access.

The bathymetry of lakes Calado (73 km^2; Lesack & Melack, 1995), Lago Grande de Curuai (2440 km^2; Barbosa et al., 2006) and Janauacá (786 km^2; Pinel et al., 2015) were estimated in situ, allowing the implementation of local two-dimensional models and expanding the knowledge regarding the hydrology of river-floodplain systems (Bonnet et al., 2008, 2017; Ji et al., 2019; Lesack & Melack, 1995; Pinel et al., 2019; Rudorff et al., 2014a, 2014b). Floodplains' water residence times estimated by local models range from 19 to 74 days (Bonnet et al., 2017; Rudorff et al., 2014a). In Lake Calado, local runoff represents the dominant source of water input with 57% (Lesack & Melack, 1995), so that the maximum volume of river water in the lake occurs before the river flood due to local contributions from the basin in this period (Ji et al., 2019). On the other hand, the main water input comes from the river in Lago Grande de Curuai and Lago Janauacá, representing, respectively, 77% (Bonnet et al., 2008) and 93% (Bonnet et al., 2017) of the total water sources. Rudorff et al. (2014b) showed that overbank flow in the Curuai floodplain accounts for 93% of the total flow in the river-floodplain direction and 54% of the flow in the opposite direction (floodplain-river), with the remaining flow being channelized. These lakes illustrate the heterogeneity in river-floodplain hydrodynamics in Amazon floodplain systems. Moreover, water fluxes in these systems were not described in most studies. The first (and only, to our knowledge) validation of water velocity in an Amazonian floodplain was performed by Pinel et al. (2019) for Lake Janauacá. Therefore, there is still a gap in knowledge about the understanding of this complex and important systems.

The accuracy of the models used to understand the detailed hydrodynamics of the floodplain over an extensive region is limited by the topographic data. On the one hand, accuracy is limited by the quality and resolution of global DEMs in regional applications, and on the other hand, the study area is limited by in situ bathymetry, as in local models. To overcome this limitation, Fassoni-Andrade et al. (2020a) estimated the topography of a large reach of the Amazon River floodplain (~40,000 km^2) at 30 m resolution using remote sensing data. Although topography has not been estimated in permanently flooded areas of channels and lakes in the floodplain, this dataset presents a unique opportunity to investigate the bidirectional flows and the river-floodplain water exchange over a large floodplain area using a two-dimensional hydraulic model with better topographic representation than global DEMs. Therefore, the goal of the present study is to apply a hydraulic model in the central floodplain Amazon using this dataset, in order to describe the floodplains hydrodynamics of hydrological years characterized as normal (2008), intense (2009), and weak (2010) flood conditions.

The study is divided into methodology (Section 2), validation (Section 3), results (Section 4), and conclusions (Section 5). At the beginning of sections 3 and 4 we synthesize in topics the lessons learned about the modeling and the system hydrodynamics to highlight the main results.

2. Data sets and methods

2.1. Hydraulic model and simulation domain

Recent advances from the HEC-RAS model allows the representation of two-dimensional flows from the numerical solution of the shallow water equations. It represents the inertia terms, pressure gradient and gravitational effects, friction, turbulence, and Coriolis effects. Details of the formulations and numerical schemes used in the model (6.0.1 version) can be found in Brunner (2016).

The model was applied to 1100 km reach of the Amazon River between the confluence of the Negro and Xingu rivers, where an extensive floodplain is present (Figure 1). The computational domain, which covers ~40,000 km^2, was delimited from a 1 km buffer of the Amazon wetlands mask (Hess et al., 2015; Figure 1).

The simulation covered 3 hydrological years (November 2007 to October 2010), that comprises normal (mid-2008), intense (mid-2009) and weak (mid-2010) flood conditions (Filizola et al., 2014). An initial period of 5 months was considered as model initialization, allowing the filling of the floodplain before the evaluated period.

The time series of Amazon discharge from the Manacapuru station, located ~67 km upstream of the domain upstream limit (Figure 1), was used as a boundary condition of the Amazon River. Detailed information for this and other stations operated by the Agência Nacional de Águas e Saneamento Básico (ANA; snirh.gov.br/hidroweb/serieshistoricas) are shown in Table S1 in supporting information. Downstream, water level time series from the Porto de Moz station (operated by ANA) was used, which represents the water level of the Xingu River at its confluence with the Amazon River, located ~77 km downstream from the domain (Figure 1). Due to the backwater effect on the Amazon River tributaries, the station can be representative of the Amazon River level. The vertical levelling of this station (EGM 2008) was done considering the altimetry level at a nearby virtual station of Sentinel-3A satellite (station amz_amz_s3a_0433_01; hydroweb.theia-land.fr/) with an estimated bias of 1.108 m (49 data). Tidal effect from water level was filtered using a moving window of 28 days.

The discharges of the main tributaries in the domain were considered as boundary conditions from simulated data performed by Siqueira et al. (2018) using the MGB hydrological model (Collischonn et al., 2007). For this, 12 tributaries that intersect with the computational domain were selected as they represent up to 99% of the average modeled flow contributing to the computational domain (see Figure 1).

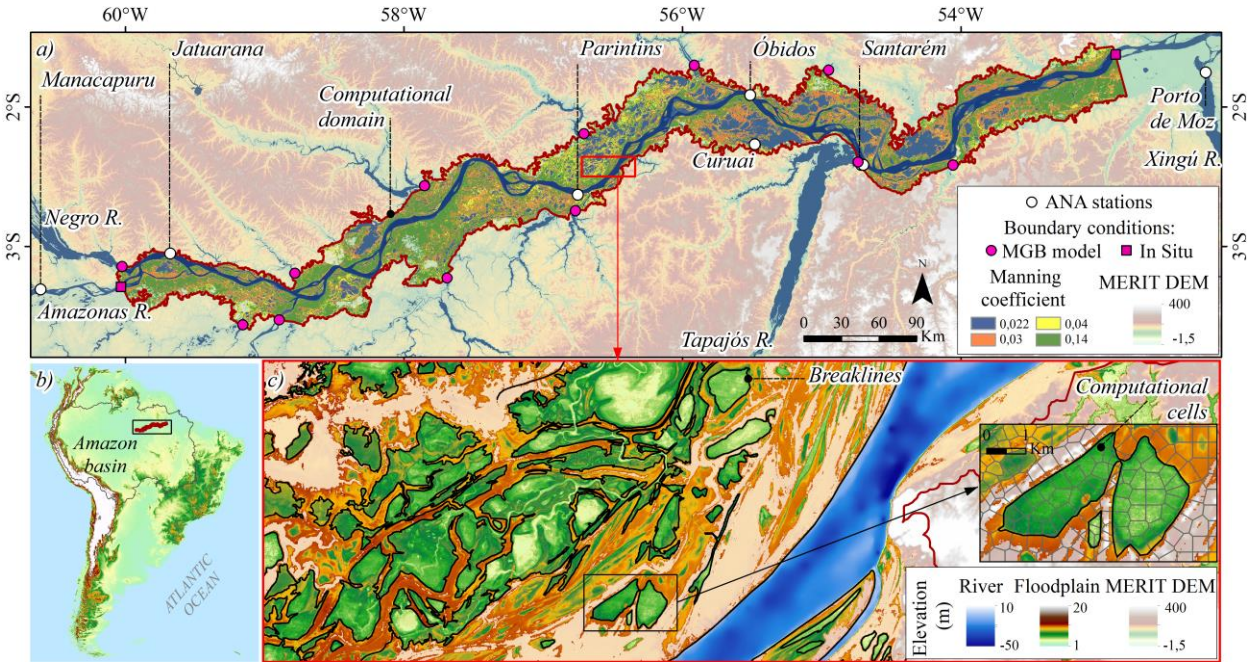

Figure 1. a) Location of computational domain (~40,000 km^2), boundary conditions and ANA stations. Manning coefficient mapping (within boundary) and topographic model MERIT DEM (outside boundary). b) Location of the central region of the Amazon basin. c) Detail of the floodplain topography, position of computational cells and breaklines used in the model.

2.2. Topography and computational mesh

A composite topography map was produced by merging several databases. In the Amazon River and open water areas of the floodplain, the topography estimated by Fassoni-Andrade et al. (2020a) at 30 m spatial resolution was used (Figure 1a; available at data.mendeley.com/datasets/vn599y9szb/1). This mapping was created by digitizing nautical charts for the rivers, and using the Flood2Topo method (Fassoni-Andrade et al., 2020b) via optical satellite data representing the topographic variation of lakes and narrow channels in the open water regions of the floodplain. Validation using locally derived bathymetry showed a root mean square error (RMSE) of 90 cm for the floodplain bottom level. However, the bathymetry of deeper regions in the floodplain, which are always flooded, is underestimated since it represents the lowest observed water level in 30 years. The average bias of the river bathymetry, documented as 5 m (Fassoni-Andrade et al., 2020a), was discounted in the elevation values.

In the flooded vegetation and upland areas, topography was obtained using MERIT DEM v1.0.1 (Multi-Error-Removed Improved-Terrain DEM; available at hydro.iis.u-tokyo.ac.jp/~yamadai/MERIT_DEM/). This terrain elevation model was chosen because it has global coverage and comprises a removal of absolute bias, noise, and vegetation height from SRTM3 DEM and AW3D-30m v1 data (Yamazaki et al., 2017). The vertical reference of the model (EGM 1996) was adjusted to the EGM 2008 model using the MSP program GEOTRANS 3.7 (available at: earth-info.nga.mil/GandG/geotrans/index.html#zza1).

HEC-RAS model uses an unstructured computational mesh in which the orientation and size of the cells can vary according to topographic variation, so that breaklines can be included to

define the orientation of the computational cell faces. Thus, breaklines were added (e.g., Figure 1d) considering a manual digitization of the topographic contours of the river banks and in floodplain based on the isolines formed by the 90% and 60% flood frequency of the flood frequency map elaborated by Fassoni-Andrade et al. (2020a). These thresholds (90% and 60%) roughly delineate the location of greater topographic variations, such as riverbanks. The computational mesh generated with a nominal cell size of 400 m (detailed representation through breaklines in smaller features) resulted in ~260,000 cells. Despite the nominal size of 400 m, smaller features were represented through the breaklines considering the 30 m topography.

2.3. Manning's roughness coefficient

Manning's roughness coefficient map in the floodplain (Figure 1) was prepared based on the Amazon wetland land cover mapping of Hess et al. (2015). Manning's values were assigned for each class based on recommendations by Arcement Jr.; Schneider (1989) e Chow (1959), according to Table S2. More bathymetry, water velocity and level data in the floodplain would be needed for manning calibration in the floodplain, with possibly weak impacts on the quantitative conclusions of this study.

Manning's value in the Amazon River was calibrated for the period from September 1, 2006, to August 31, 2007 (1 year). The lowest RMSE of the water level simulated and observed at the stations at Jatuarana (0.19 m), Parintins (0.13 m) and Santarém (0.21 m; ANA operated stations; Location in Figure 1) resulted from a Manning coefficient of 0.022. Lefavour and Alsdorf (2005) assumed a Manning coefficient of 0.025 with an error of 12% for discharge estimation in the Solimões River considering a sand channel without vegetation. Wilson et al., (2007) calibrated a regional hydraulic model of the lower Solimões River using values in the range between 0.022 and 0.028 based on the estimation of Lefavour and Alsdorf (2005). Therefore, although the value found is low compared to values of Rudorff et al. (2014a; 0.031) and Trigg et al. (2009; 0.032) it is within the uncertainty bound considered by Lefavour and Alsdorf (2005).

2.4. Modelling performance metrics

The hydrodynamic model was validated against in situ and satellite observations to access its capability to represent the flooded areas, water surface elevation and water flows in river and floodplains.

Several remote sensing-derived Amazon flood extent databases have been developed in recent years to characterize flooding in Amazon (Fassoni-Andrade et al., 2021). This is not a trivial mapping and the different approaches have led to disagreements, as shown by the comparison documented in Fleischmann et al. (2022). We used two basin-scale databases that consider periods of maximum and minimum inundation (Hess et al., 2015; Rosenqvist et al., 2020). The Hess mapping (hereafter called HESS) (Hess et al., 2015), one of the most widely used in the validation of hydrologic-hydrodynamic models in the Amazon basin, depicts wetland inundation and vegetation for the central Amazon basin based on JERS SAR imagery for the flood and low-water periods - May 1996 and October 1995 (available at https://daac.ornl.gov/LBA/guides/LC07_Amazon_Wetlands.html). Rosenqvist's mapping (hereafter called ALOS) (Rosenqvist et al., 2020), on the other hand, considers the maximum and

minimum flooding of 3 most recent hydrological years derived from the ALOS-2 SAR data: 2014-2015, 2015-2016 and 2015-2017 with 50 m spatial resolution (available at https://www.mdpi.com/2072-4292/12/8/1326). These mappings do not correspond to the simulation period (2006-2010), so three simulated periods of low water (November 1, 2007, 2008, and 2009) and high water (May 1, 2008, 2009, and 2010) were compared with these mappings. For this purpose, the fit metric (F, Equation 1) was used to determine the accuracy of the model (Schumann et al., 2009).

$$F = \left(\frac{a}{a+b+c}\right) 100 \quad (1)$$

where a represents the total inundated area correctly mapped by the model, b is the inundated area not mapped by the model (underestimate), and c is the area not inundated and mapped by the model (overestimate).

The water surface elevation records observed in situ at Óbidos and Curuai stations were considered for model validation (ANA operated stations; Location in Figure 1). In addition, satellite altimetry data from virtual stations spread along the river from the JASON2/JASON3 and ENVISAT satellites were also considered. These virtual stations are located at intersections of the altimeter track with the river and are available at hydroweb.theia-land.fr (Silva et al., 2010). Information for these stations can be found in Table S1. The metrics evaluated were: i) RMSE, ii) Bias, iii) Pearson correction coefficient (r), and vi) Nash-Sutcliffe efficiency coefficient (NSE).

Finally, the water flow of the Amazon River was evaluated at Óbidos (the lowermost hydrological gauge station in the Amazon basin) and at the Curuai floodplain. The Óbidos station continuously provides water level data and some flow measurements, in addition to the rating curve. Since no flow was measured between 2006 and 2010 at Óbidos, we used the rating curve for model validation, which may have large uncertainties (Filizola et al., 2014). In addition, we were able to obtain flow measurements in the Curuai floodplain during the 2006 flood season using a SonTek 1.5 MHz Mini Acoustic Doppler Current Profiler (ADCP) with errors smaller than 3%. Moving boat measurements were carried out with the Mini ADCP assembled on a home-built Catamaran platform integrated with a GPS. The ADCP platform was placed on the left side of the boat, near the bow, to avoid interference from the boat engine on measurements. The boat speed ranged from approximately 0.05 to 0.2 m s^{-1}. The same metrics for the water level were considered to evaluate the water flow.

3. Validation

3.1. Flood extent

Modelling lessons: 2D high resolution model improved the representation of flood extend compared to past modelling studies in the Amazon. Model accuracy for flood extent is usually better at high water than low water. Errors may be related to topography, local precipitation and evapotranspiration, and uncertainty of remote sensing maps.

Table 1 shows the total flood extent area mapped for the ALOS and HESS products. The area estimated by the ALOS product is 30 to 50% smaller than the area from HESS product. The interannual variability of the flood extent from the ALOS product hardly shows any difference between the years 2014 and 2017 (Table 1).

Table 1 also presents the fit metric used to compare the simulations considering low and high water periods for the three years simulated. The model performance was higher during the high water period (up to 60%) compared to the low water period (~50%). Although the metrics for both products are similar at low water, there are many more areas of simulated overestimation with the ALOS product compared to the HESS product (see green areas in Figure 2a). This is similar during the high water period (see green areas in Figure 2b), when the metrics for the HESS product (81-82%) are better compared to the ALOS product (56-58%). There is no significant variability in the metrics among the years evaluated indicating that the discordance between the simulated years (2007-2010) and the years of observations (1995-1996 and 2014-2017) is not as significant for validation as the product considered.

Applications of hydrodynamic models to Amazon floodplains at different scales found fit metric values ranging from 23 to 51% (low water) and 70 to 81% (high water) compared to HESS mapping. Paiva et al. (2013) represented the extent of large-scale flooding in the Amazon basin from the MGB model with values of 34% at low water and 70% at high water. Wilson et al. (2007) and Rudorff et al. (2014b), in regional applications of the LISFLOOD-FP 2D model along the Amazon River reaches, found values of 23 and 51% at low water and 72 and 81% at high water, respectively. Therefore, our model represented the flood extent relatively well, with average F values of 52% in the low water period and 81-82% in the high water period against HESS product. In addition, the accuracy is of local relevance (F>0.65) according to the criteria established by Fleischmann et al. (2019).

Errors in topographic mapping and the lack of representation of processes such as local precipitation and evapotranspiration in the floodplain can be sources of uncertainties in the flood extent mapping by the hydrodynamic model, especially in the low water period. However, it is noteworthy that the various remote sensing-derived water extent databases also have large inconsistencies among them. For example, Fleischmann et al. (2022) showed that HESS and ALOS mapping tend to underestimate the maximum inundation compared to subregional remote sensing-derived products, and there are large differences in minimum inundation among the different products.

Table 1. Fit metric for HESS and ALOS products considering the low and high water periods

	Low water (November)				High water (May)			
	Flooded area	F 2007	F 2008	F 2009	Flooded area	F 2008	F 2009	F 2010
HESS	17942.38 km^2	52%	52%	52%	31277.83 km^2	81%	82%	81%
ALOS 2014-2015	8938.60 km^2	51%	50%	48%	21760.10 km^2	58%	59%	58%
ALOS 2015-2016	8130.33 km^2	46%	45%	44%	20130.50 km^2	56%	56%	56%
ALOS 2016-2017	8641.35 km^2	49%	48%	47%	20679.30 km^2	56%	56%	56%

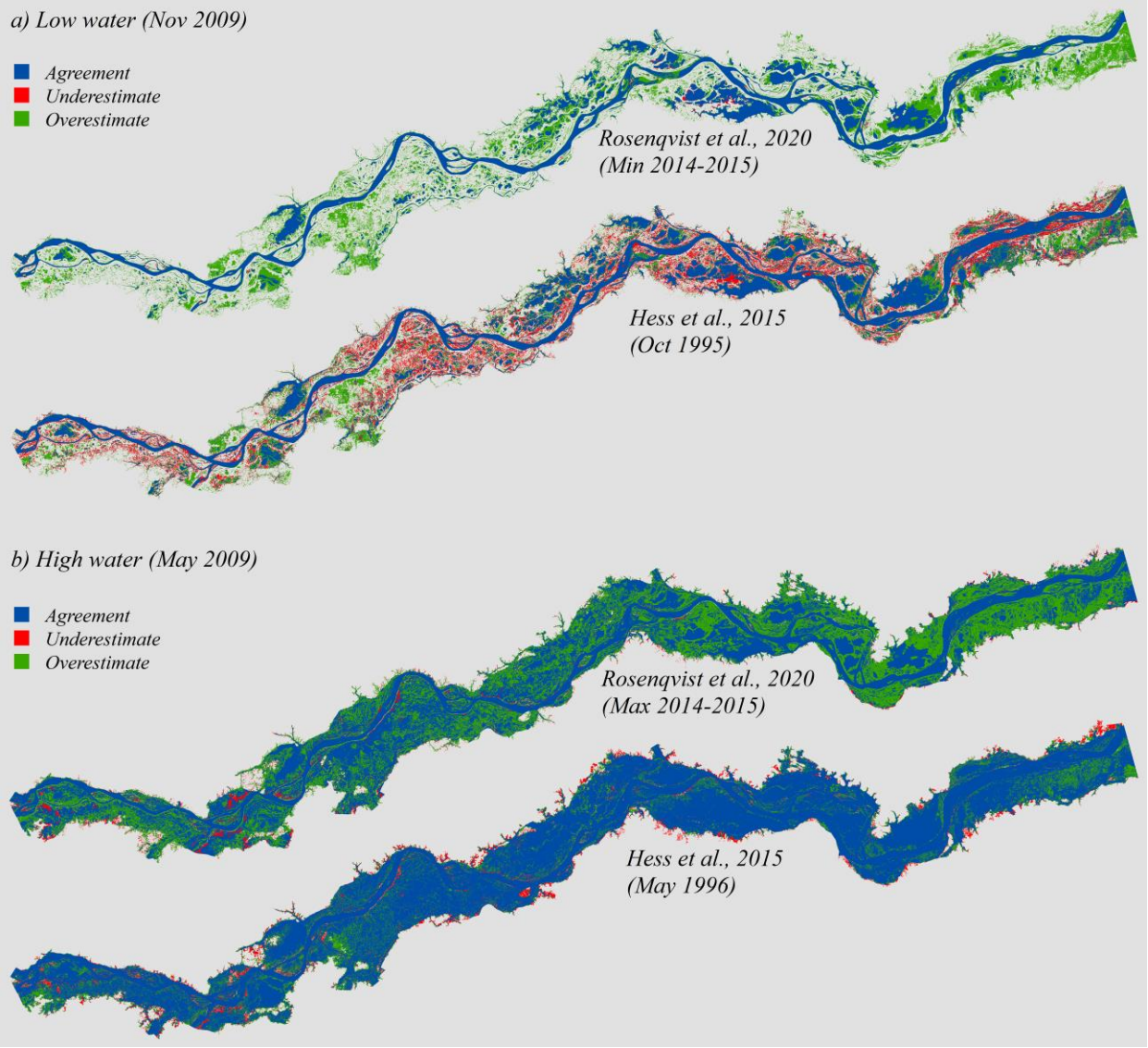

Figure 2. Flood extent mapped by the model and remote sensing products (blue), flood extent not mapped by the model (underestimate), and flood extent mapped only by the model (overestimate) considering ALOS and HESS products and simulated in November (a) and May (b) of 2009.

3.2. Water surface elevation

Modelling lessons: 2D high resolution model improves the representation of water surface elevation of the Amazon flood wave compared to past modelling studies. Error is small compared to the flood amplitude.

Absolute water surface elevation in the river was well represented in the 23 stations evaluated (Table S3), with an average bias of -0.45 m, an RMSE of 0.77 m, an NSE of 0.87, and an *r* of 0.98 (values considering the EGM 2008 model). The bias and RMSE of each station are

shown in Figure 3. Only the stations monitored by ANA agency showed a positive bias (Óbidos and Curuai), while the altimetry stations consistently showed a negative bias. The highest RMSE (1.54 m) was observed at a station located in a channel with underestimation in the low water period, as presented in Figure3b (Station 0392_01).

The errors are small in relation to the annual flood amplitude (4 to 10 m; Station 0063_01 and 0263_01 in Figure 3a) and compared to the errors found by Wilson et al. (2007), which obtained an RMSE of 0.99 m at flood and 3.17 m at low water in the Amazon River. On the other hand, Rudorff et al. (2014b) found errors of 0.27 m at the Curuai station, considering the local hydrodynamic simulation of this floodplain using observed bathymetry. Our results also have a better agreement with observations compared to large-scale modeling in the Amazon basin. For instance Paiva et al. (2013) obtained a NSE of 0.2-0.4 at Óbidos and Yamazaki, Lee, et al. (2012) obtained a NSE of 0.7 at Óbidos, where water surface elevation anomalies were evaluated.

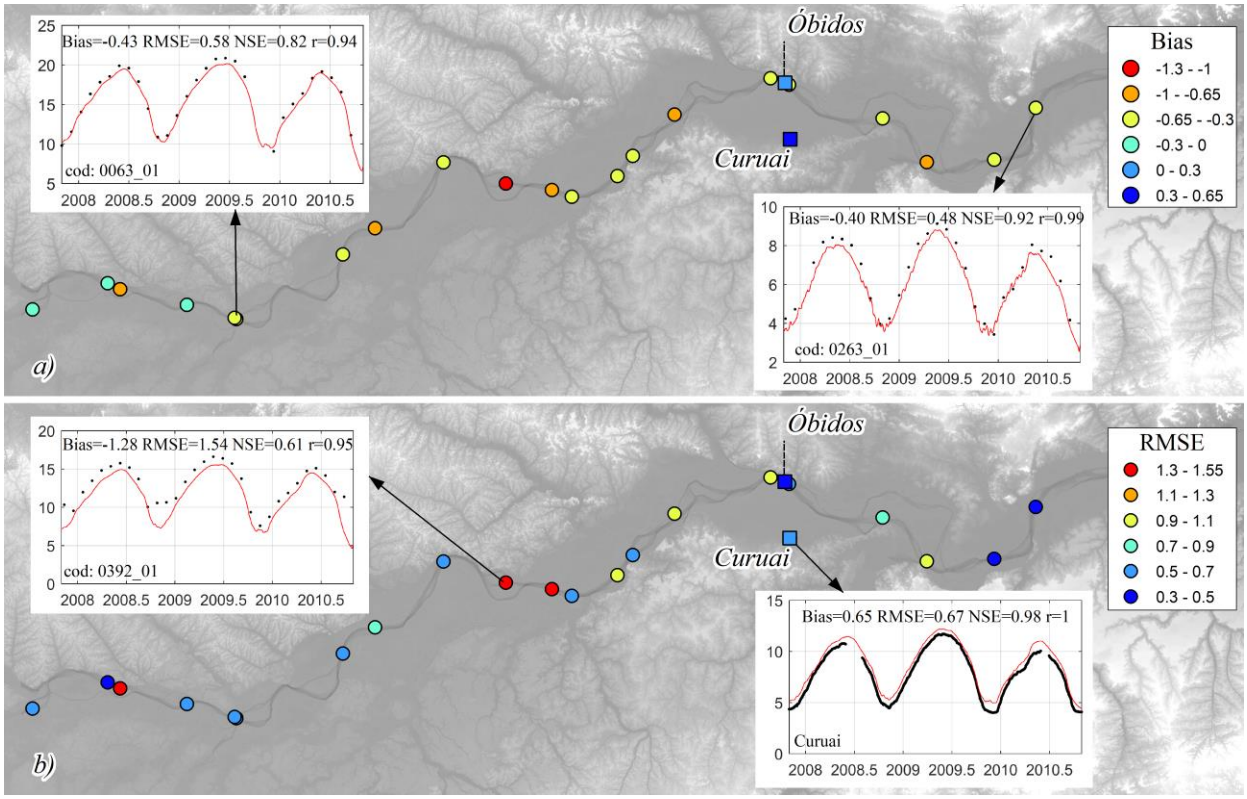

Figure 3. Validation of absolute water surface elevation derived from the model against in-situ observations of gauging stations (squares) and satellite altimetry data (circles). Spatial distribution of model performance statistics: Bias (a) and RMSE (b). Time series of the model (red line) and observed (black dots) water elevation.

3.3. River and floodplain flow

Modelling lessons: 2D high resolution model provides accurate representation of Amazon River discharge. Appropriate representation of expressive floodplain flow with errors smaller than 20%.

The Amazon River discharge at Óbidos station was adequately represented by the model with a positive bias of 1380 m^3s^{-1} (0.78% of the mean observed discharge) and an RMSE of 12713 m^3s^{-1} (7.23% of the mean observed discharge) and relatively high NSE = 0.94. The values during the rising period (February to June) were underestimated, while during the rest of the year discharge values were slightly overestimated (Figure 4a). It is likely that this underestimation is related to the uncertainties of the rating curve at Óbidos since it is calculated considering a single stage-discharge relationship. As Filizola et al. (2014) pointed out, a large amount of water goes to the floodplain during the flood, so the stage-discharge relationship may be different in this period compared to the low water period.

The observed flow was also evaluated across four transects located at the downstream outlet of the floodplain on June 26, 2006 (blue spots profiles in Figure 4b and c). In spite of the uncertainty of the bathymetry used in the simulation, the model adequately represented the flows on the floodplain, with differences from the observed flow ranging from -21% to 22% ($(Q_{mod} - Q_{obs})/Q_{mod}$). The flows in the three main channels (profiles 1, 2, and 3) were overestimated, while the flow in the longest profile was underestimated (profile 4). What is noteworthy about these measurements is the order of magnitude of the flows (ranging from 3'000 to 19'000 m^3s^{-1}). The outflow on the floodplain in profile 4 represents 8.3% of the discharge observed at Óbidos on the same day (234'000 m^3s^{-1}) and is greater than the average discharge of the Tapajós River (14'500 m^3s^{-1}).

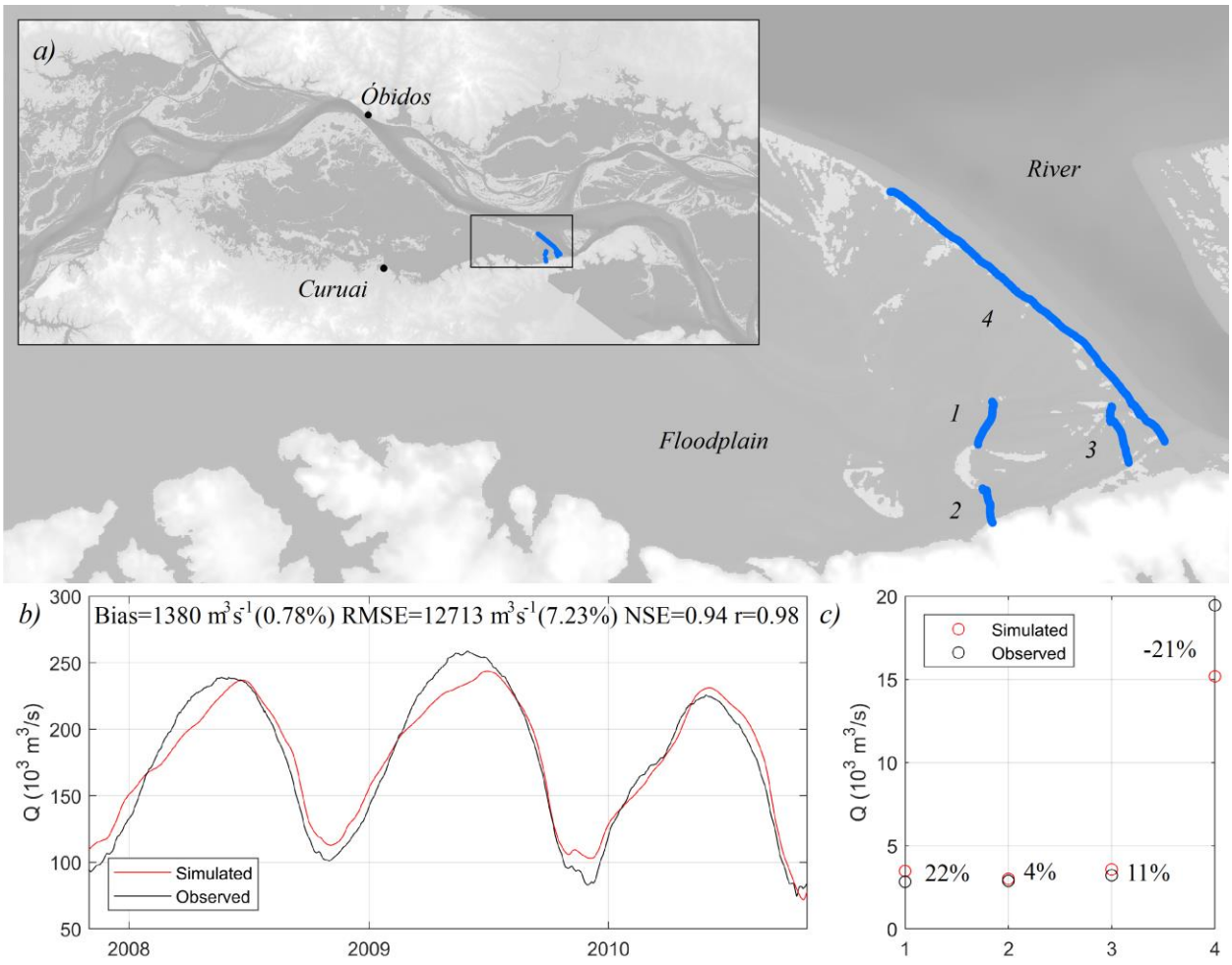

Figure 4. Validation of water flow derived from the model (red line/dot) against observation (black line/dot) at Óbidos station (a) and in the floodplain on June 26, 2006 (b and c). Blue spots indicate location of ADCP profiles (1, 2, 3, and 4).

4. Flood dynamics on the floodplain

4.1. Volume, depth, and flood extent

Lesson 1: Annual volume variation of 160 km^3 in the central Amazon floodplain. Variation represents about 3% of the Amazon River volume exported to the ocean annually. Intense and weak floods cause interannual variability of 20% in volume variation.

Lesson 2: Average water depth in the central Amazon floodplain ranges from 2.5 to 7.1 m annually. Intense and weak floods cause variations of up to 1 m at high water or 22% of the annual variation.

Lesson 3: Annual flood extent variation of 7'560 km^2 in the central Amazon floodplain. Intense and weak floods cause interannual variability of only 3% in flood extent variation. Flood extent finds a plateau in extreme floods, possibly due to topographic constrains.

Lesson 4: Significant flood extent and volume hysteresis that may be related to the floodplain hydrodynamic complexity.

The active volume stored during 2007 and 2010 in the floodplain is presented in Figure 5a. In the low water period (November), the volume stored ranged from 55.3 km^3 (2010) to 59.68 km^3 (2009), while in the high water period (June), the volume stored ranged from 204 km^3 (2010) to 238 km^3 (2009). Therefore, the floodplain has an average volume variation of 162 km^3, i.e., annually, this volume is stored and drained in the floodplain between low water and flood periods. The volume stored annually in the central Amazon floodplain (162 km^3) represents about 2.8% of the Amazon River volume exported to the ocean annually. This annual variation is larger than the estimated over the open-water floodplains of the central Amazon (116 km^3; Fassoni-Andrade et al., 2020a) and smaller than the estimate over the Amazon floodplains in six square regions of 330 km × 330 km (285 km^3; Alsdorf et al., 2010). It represents 13.5% (Papa et al., 2013) to 18% (Frappart et al., 2019) of the total surface water storage at the Amazon basin scale estimated by remote sensing data. Furthermore, the estimated volume stored in the floodplain showed a difference of 34 km^3 at the flood peak between years characterized by intense (2009) and weak (2010) flood. This volume is significant and represents 20% of the annual volume variation and 60% of the average volume stored in the floodplain during the low water period.

The water depth in the floodplain showed a similar pattern to that of the stored volume (Figure 5b), with an average depth of 4.62 m, i.e., the average depth ranges from 2.5 m to 7.12 m between the low water and high water periods. The average depth variation in the flood period was 40 cm lower in the dry year (2010) and 60 cm higher in the wet year (2009) compared to a normal year (2008). These values can be significant when considering the amplitude of the water level, which varies from 10 m upstream to 4 m downstream reach (Fassoni-Andrade et al., 2020a). Furthermore, the variation of 1 m between extreme floods (2009 and 2010) represents 22% of the annual variation of the average depth.

The flood extent showed an average value of 31'500 km^2 and 23'940 km^2 during the high water and the low water periods, respectively (Figure 5c), i.e., an annual variation of 7'560 km^2. These values represent, respectively, 5% and 8% of the mapped wetlands in the Amazon basin during the high and low water periods (Hess et al., 2015). However, in contrast to the strong interannual variation in stored volume, the flood extent presented a plateau during the high water period with differences of ~200 km^2 between 2009 and 2010, which represents only 2.6% of the average variation between high and low water periods. This means that flood intensity does not have such a large impact on flood extent (2.6%) compared to its impact on volume (20%) and on water depth (22%). The flood extent finds a plateau during the flood possibly due to topographic constrains limited by the geomorphology of the Amazon River and the Uplands (Terras Altas) at the floodplain boundaries

The relationship between volume and flood extent on the floodplain indicates a counter-clockwise hysteresis, as also documented by Rudorff et al. (2014b) for Curuai floodplain, i.e., for the same stored volume, the flood extent is larger in the falling than in the rising period (Figure 5d). For example, the flood extent was 30'000 m^2 in the falling period and 28'000 m^2 in the rising period for a stored volume of 100 km^3. This may be related to the floodplain hydrodynamic complexity, as the asymmetry of the Amazon River hydrograph, where the rising period is slower than the falling period (Fleischmann et al., 2016), the reversal of river-floodplain surface water slope (Zhang & Werner, 2015), or the time taken for water to fill deeper parts of the floodplain before flooding upper regions.

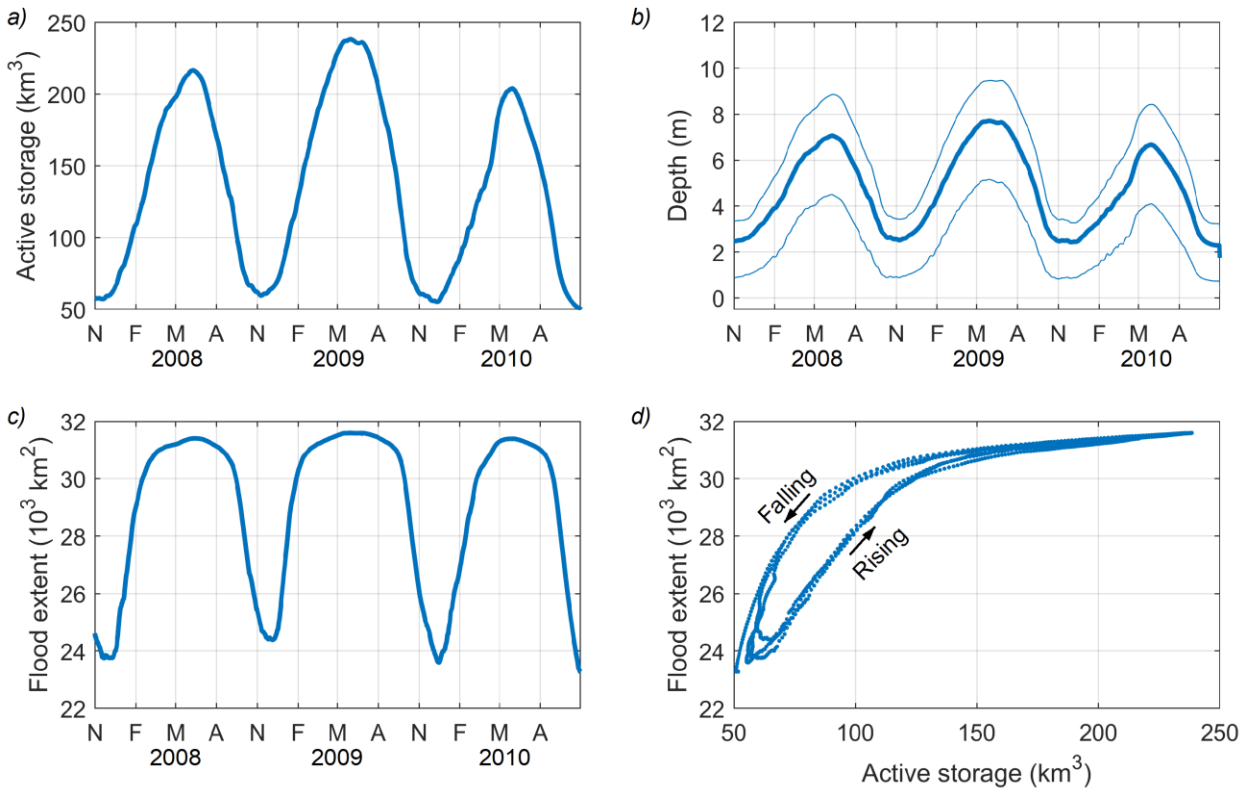

Figure 5. Temporal series of a) active storage, b) average depth ± 25 and 75 percentile and c) flood extent in the floodplain. d) The relationship between active storage and flood extent in the floodplain.

4.2. River-floodplain flows exchange

Lesson 5: Central Amazon floodplain is fragmented into floodplain units of ~80 km with expressive water inflow/outflow from/to the main river.

Lesson 6: Extreme floods can offset by one month the timing of the floodplain inflow onset (delay and advance). No interannual variability in the timing of the maximum flood.

Lesson 7: Gross floodplain inflow and outflow greatly surpass the net inflow and outflow, indicating that the floodplain flux is generally more expressive than storage infilling and outfilling.

Lesson 8: Variations in flood duration in extreme floods can induce a 33% (22%) increase (decrease) in floodplain inflow.

The water exchange between the Amazon River and the floodplain was evaluated in eight units by estimating the flow across transects parallel to riverbanks. In each unit, two transects of equal length (L) were defined: one upstream and one downstream. These transects consider that most of the water inflow (outflow) in the floodplain occurs in the upstream (downstream) half, however dominant inflow/outflow boundaries have not been defined. In the Curuai floodplain (Unit 6), for example, water outflow is predominantly in a smaller downstream transect (Rudorff et al., 2014a). Figure 6 shows the flows across both transects (blue and yellow), and the resulting

net flow (red line). Positive values indicate that the floodplain is receiving water from the river, and negative values indicate that water is flowing out of the floodplain. Once our model does not consider infiltration, precipitation, and transpiration processes in the domain, the net flow is the result of the discharge received from the tributaries.

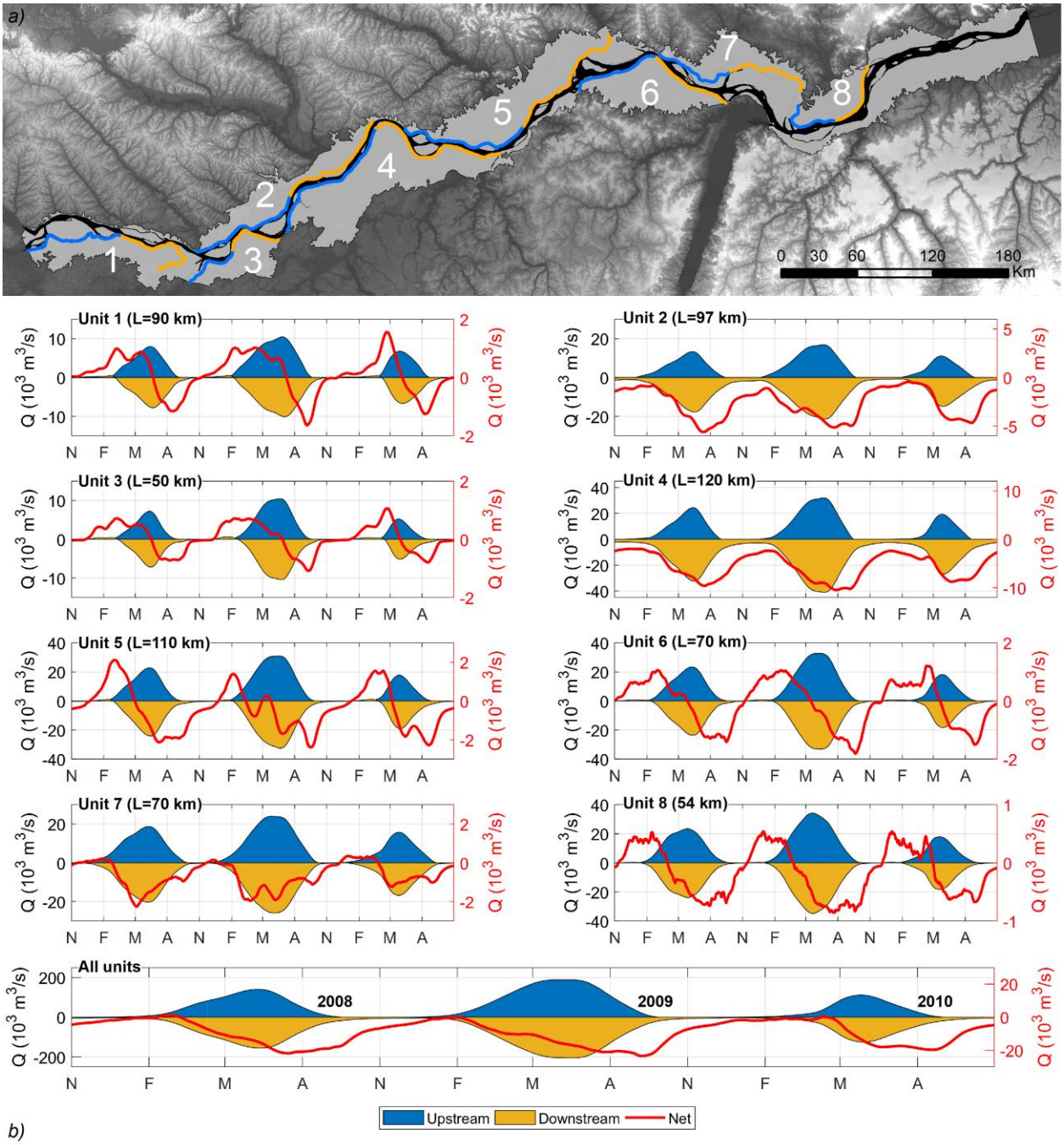

Figure 6. (a) Map and (b) temporal series of water flow in eight floodplain units from 2008 to 2010. Blue and yellow transects represent, respectively, the upstream and downstream region of

each unit (left y-axis), and the red line represents the resulting net flow (right y-axis). Note the widely different scales in left and right y-axes.

In all units, the inflow and outflow of water from the floodplain predominates, respectively, in the upstream and downstream transect, i.e., inflow or outflow can occur in both transects, but the balance is positive (negative) for the upstream (downstream) transect. In general, the positive water inflow balance in the floodplain begins with the river flood and predominates until the flood peak (May/June/July). During the falling period, outflow becomes predominant with a maximum in August/September, when there is little or no inflow to the floodplain. Negative balance (floodplain flow into the river) continues to occur in the units with small values until the onset of the flood. However, in regions 2 and 4, this flow from the floodplain to the river is greater in the low water period because there is a significant flow contribution from the tributaries.

In units 1, 3, 5, and 6, flooding begins between February and April, depending on the year: March in 2008, February in 2009, and April in 2010. That is, a weak flood and an intense flood cause, respectively, a delay and an advanced of the water inflow into the floodplain by approximately one month in these units. These findings are similar to results for Lake Janauacá in central Amazon (Pinel et al., 2019). Inflow onset in units 2, 4, 7, and 8 occurs in December/January regardless of the year, therefore, these areas seem to have more connection with the river from channelized flows. Although the positive balance is initiated in different months in the units, the maximum inflow and outflow occurs at the time of river peak flood (June/July), since diffuse overbank throughflow in the floodplain predominates.

The water exchange between the river and the floodplain during the flood is very intense with inflows and outflows ranging from 5'500 to 35'000 m^3s^{-1} (units 3 in 2010 and 8 in 2009, respectively). However, these values represent the inflow and outflow of water occurring practically at the same time in the units, i.e., gross floodplain inflow and outflow greatly surpass the net inflow and outflow, indicating that the floodplain flux is generally more expressive than storage infilling and outfilling.

The total water inflow considering all units (area of 40'000 km^2) is maximum during the 2009 flood with values of 189'600 m^3s^{-1}, representing more than the flood peak of the Solimões River in the same year (~160'000 m^3s^{-1}). On the other hand, the outflow from the floodplain is 206'000 m^3s^{-1} in the 2009 flood. These values are much lower at the peak of the 2010 weak flood: the maximum inflow and outflow are respectively to 60% and 62% of the values in 2009. Therefore, an intense (weak) flood promotes a 33% (22%) increase (decrease) in floodplain inflow during the flood compared to a more normal year (e.g., 2008, when 142'700 m^3s^{-1} are seen).

4.3. Riverine fluxes over floodplain units

Lesson 9: Amazon floodplain units work as a river with flows up to 20% of the Amazon River discharge.

Lesson 10: Heterogeneity in floodplain velocity fields with floodplain channels of active flow and storage areas.

Figure 7 shows the transverse flows across the sections in the floodplain units (purple; left y-axis) and this flow (Q_F) expressed as a percentage of the Amazon River discharge (Q_R; right y-axis) for 2008, 2009, and 2010.

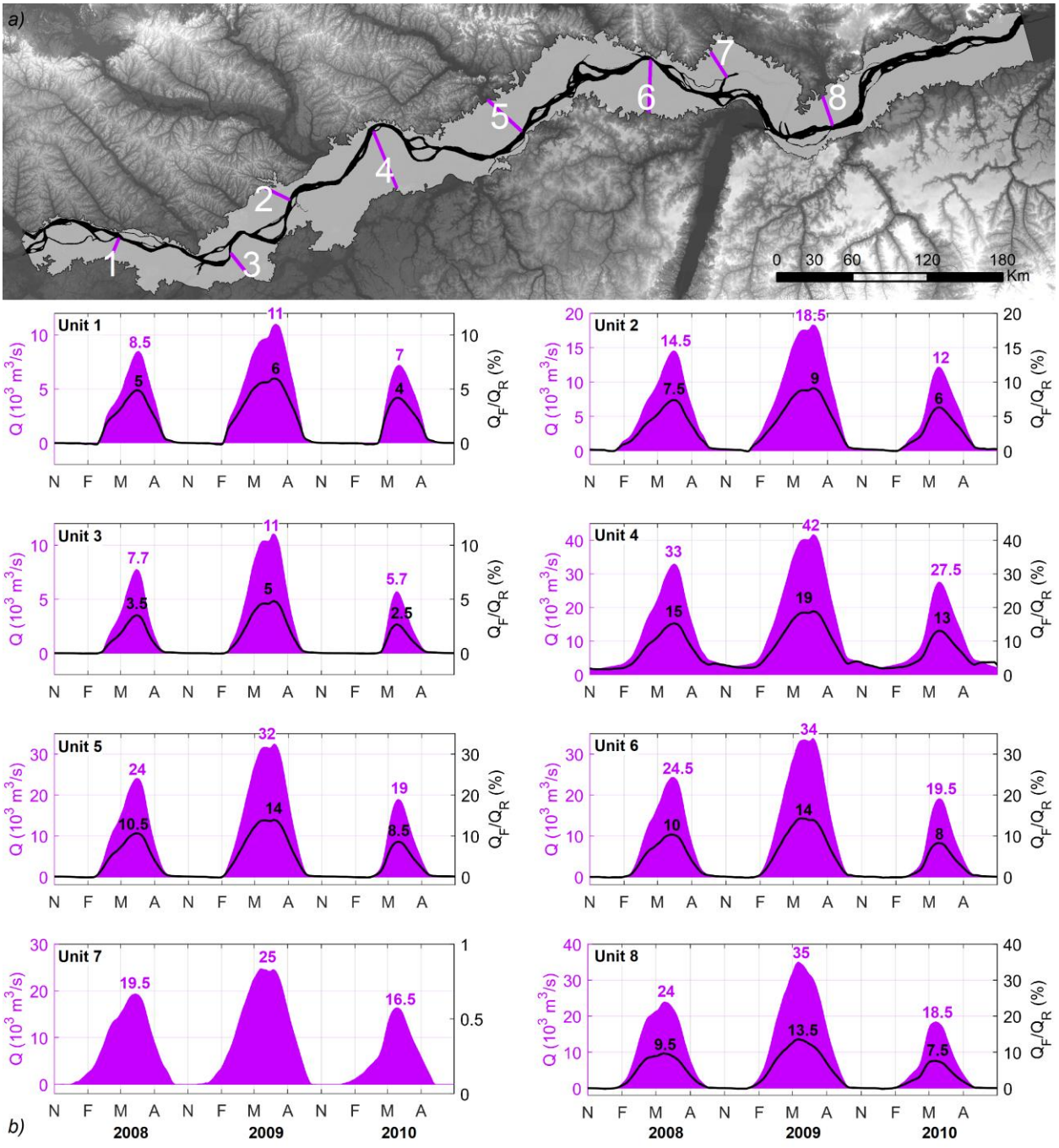

Figure 7. (a) Map and (b) temporal series of transverse flows in the floodplain in the eight units (purple; left y-axis) and the percentage of flow in the transverse transect (Q_F) relative to the river discharge (Q_R) (black; right y-axis) from 2008 to 2010.

Flows along the transverse profiles are towards downstream during the flood (positive values in the graphs) and broadly parallel to the river, as can be seen in Figure 8 for the 2009 flood. During 2008 (normal year), floodplain flows vary from 7'700 to 33'000 m^3s^{-1} (units 3 and 4) representing from 3.5% to 15% of the Amazon River discharge (average of 8.7%). During intense and weak floods, flows vary from 5% to 19% (2009) and from 2.5% to 13% (2010) of the Amazon River discharge, respectively. These values are very significant, as they are similar in magnitude to the average discharge of the largest tributaries of the Amazon River (e.g., 28'000 m^3s^{-1} for the Negro River and 31'000 m^3s^{-1} for the Madeira River). As these flows are not stored in the floodplain (inflow and outflow occur roughly at the same time; Figure 6), the eight units behave as very active zones with riverine fluxes during the flood. Furthermore, the Amazon River can be considered not only as the most voluminous river in the world (Callède et al., 2010) but also as the widest during the flood (ranging from 21 km to 54 km wide), since the floodplain units can be considered as an active extension of the river. Velocity fields (Figure 8) in the floodplain are heterogeneous with storage areas, which may be disconnected from the Amazon River, and active flows in channels.

During the low water period, the flow in the cross transects is significantly weaker and may occur in the opposite direction, towards upstream. These reverse flows in February 2009, for example, ranged from 76 m^3s^{-1} to 389 m^3s^{-1} (units 3 and 6). This is also observed in the downstream transects (Figure 6), i.e., there is an inflow in the floodplain in the downstream region during the low-water period, predominantly in February.

The estimation of the amount of water exchanged between the Amazon River and the floodplain is not a consensus. From the water balance of six regions along the Amazon River using remote sensing observations, Alsdorf et al. (2010) showed that the filling or drainage of the floodplain accounts for no more than 10% of the river discharge during any time in the regions evaluated. On the other hand, Richey et al. (1989) estimated that up to 30% of the Amazon River discharge is exchanged with the floodplain using water balance and a simplified routing propagation method (Muskingum-Cunge). Getirana et al. (2012) showed much lower values using a global-scale flow routing scheme, with a mean of 2.3% and a maximum of 4% in central Amazon. Our findings showed that from 3.5% to 15% of the Amazon River flow passes through the floodplain during a moderate flood but can reach 20% during an intense flood. Therefore, our results are larger and lower than to Gentirana's and Richey's estimates, respectively, however, the two-dimensional hydrodynamic modeling approach performed in this study is the only one that allowed direct estimates of gross floodplain flows.

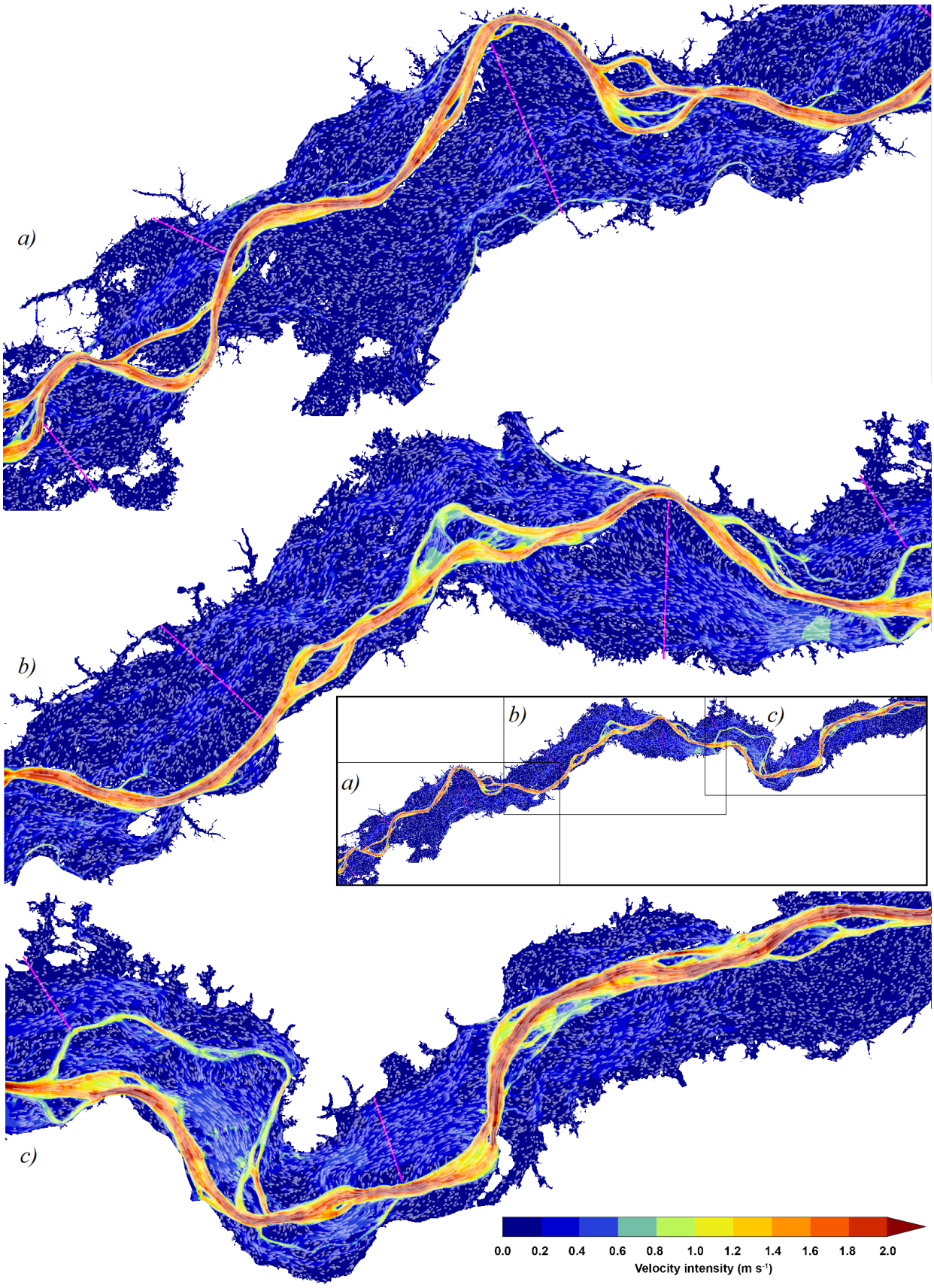

539

Figure 8. Map of water velocity field in the floodplain during the flood period (June 15, 2009). The blue to red colorbar indicates the velocity intensity (m s^{-1}) and the white streamlines the flow direction. The panels are a continuous sequence of the study area, as seen in the inset.

4.4. Residence time

Lesson 11: Water renewal in the floodplain units is high (low) during high water (low water) with water residence time around 6 days during high water and several months during low water period.

Lesson 12: Floodplains connectivity increases from upstream to downstream of the Amazon River.

Lesson 13: Intense and weak floods cause variations of up to 80 days in the duration of the period of high connectivity.

Water residence time in the floodplain units was calculated by the ratio of water volume to net flow, which represents a condition at a given instant, i.e., high values represent a theoretical steady-state condition that does not actually occur, since the inflows and outflows are dynamic in the floodplain. The residence time can be clearly divided into two periods in the eight units: one of high connectivity of the floodplain with the river during the flood (gray regions in Figure 9) and one of low connectivity during the low water. Water renewal in the flood season (April/May/June) is high with residence time values ranging from 1.5 to 13 days (units 8 and 1, respectively) with an average of 6.4 days for all units. After the flood, residence time increases rapidly in the falling period (August/September/October) to values greater than 100 days at low water (November to January), except for units 2 and 4. In these units, residence time at low water remains shorter, as it varies between 50 and 75 days due to the greater contribution of tributaries. These estimates are global at the scale of the floodplain units, but the residence time may vary within a given floodplain, especially in the low water period, among regions of swift current, such as channels connected to the river, and slower flow regions, such as lakes disconnected from the drainage network.

The duration of the high connectivity period, defined here as the period in which the residence time is less than or equal to 25 days (gray regions in the Figure 9), has an average of 177 days in all units. In units 1, 3 and 5, the duration of high connectivity varies between 100 and 150 days. In units 2, 4 and 6 the duration is 150 to 200 days, and in units 7 and 8 the duration is 200 to 250 days. Therefore, there appears to be an increase in floodplains connectivity from upstream units to downstream units.

The mean residence time in 2008 was 6.4 days with the high connectivity period lasting 6 months (179 days), whereas in 2009 and 2010, the mean residence time was 5.4 and 7.4 days with high connectivity during 215 and 137 days, respectively. Thus, an intense (weak) flood appears to promote a shorter (longer) average residence time of approximately 1 day and a longer (shorter) high connectivity period between the river and the floodplain of approximately 40 days. This is in line with section 4.2, in which an intense (weak) flood causes an advanced (a delay) of the water inflow into the floodplain by approximately one month.

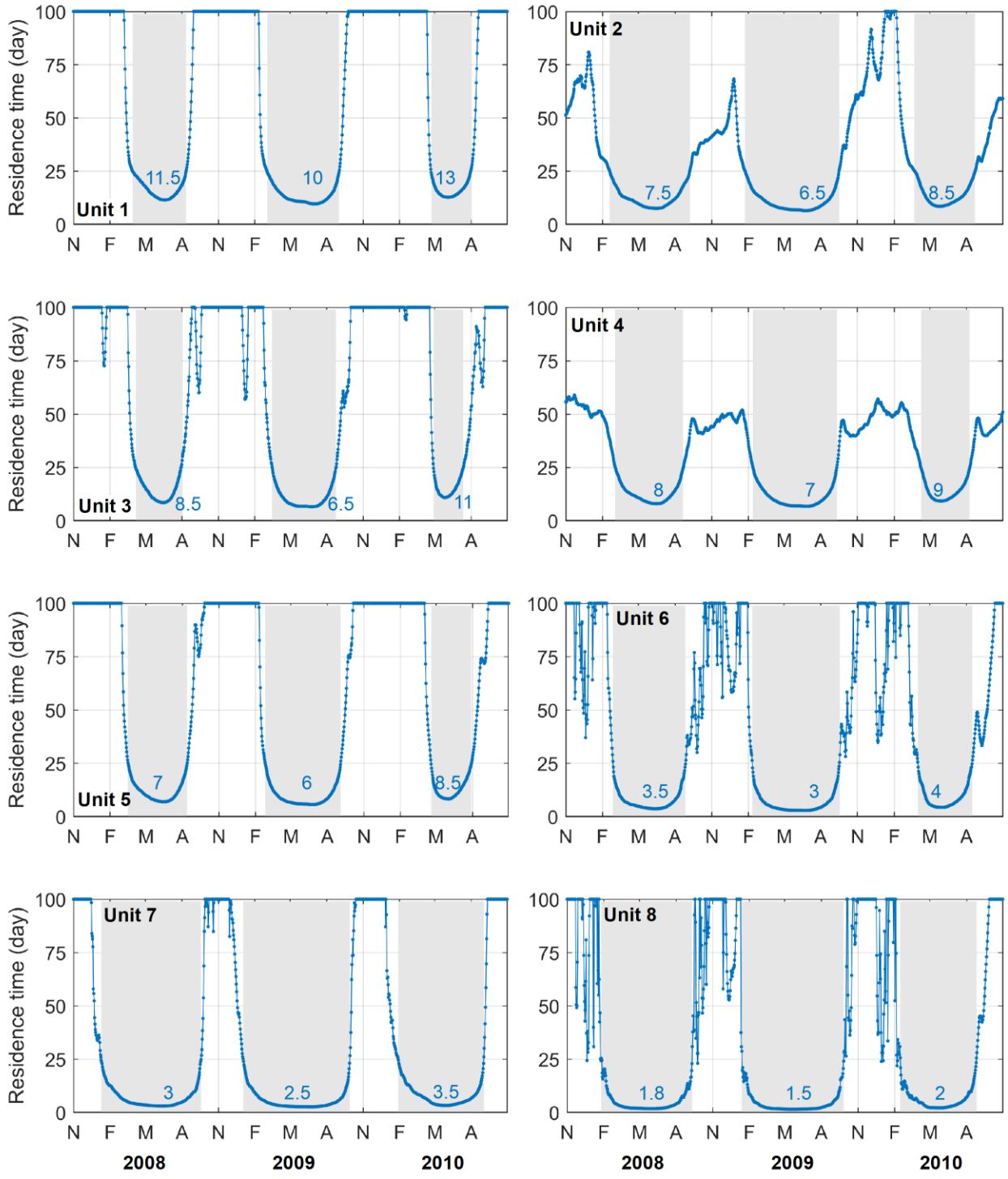

Figure 9. Temporal series of water residence time in the eight units from 2007 to 2010 (restricted to values smaller than 100days for clarity). Blue labels represent the minimum observed during the flood and gray regions represent the high connectivity period, defined as the period in which the residence time is less than or equal to 25 days.

5. Summary and conclusions

In this study, a hydrodynamic simulation of water flows in the central Amazon floodplain was performed for the first time considering a 2D hydrodynamic model and a large area (40'000 km^2) with detailed topographic information (30 m of spatial resolution). High resolution 2D model improved the representation of water surface elevation of the Amazon River and flood extent in the floodplain compared to past modelling studies. Model accuracy for flood extent is usually better at high water (~80%) than low water (~52%) and the error in water surface elevation (77 cm) is small compared to the Amazon flood amplitude. The model also provides accurate representation of floodplain flow and Amazon River discharge with errors smaller than 20%.

Part of the modelling errors may be related to topography, local infiltration, precipitation an evaporation, and uncertainty of remote sensing maps (water extent). Despite the small error of the topographic data (90 cm), the permanently flooded areas in the floodplain are underestimated causing uncertainties in these areas in our modeling (depth and volume), especially in the low water period. The representation of hydrological processes in the floodplain can be evaluate in future studies since these processes can affect the residence time and water flow in the floodplain (e.g. Tull et al., 2022).

The stored volume, average depth, and flood extent in the floodplain varied on average 162 km^3, 4.6 m (2.5 to 7.1), and 7'560 km^2 between the low and high water periods (*Lessons 1, 2, 3*; hereafter *L*). The floodplain can be compared with a confined basin in which intense or weak floods, such as that of 2009 and 2010, have more impact on the stored volume and water depth in the floodplain than on the flood extent (*L3*). We observed significant flood extent and volume hysteresis that may relate to in the floodplain hydrodynamic complexity (*L4*).

Central Amazon floodplain is fragmented into floodplain units of ~80 km with expressive water inflow/outflow from/to the main river (*L5*). Gross floodplain inflow and outflow greatly surpass the net inflow and outflow, indicating that the floodplain flux is generally more expressive than storage infilling and outfilling (*L7*). Intense and week floods can promote an advance and delay, respectively, of up to one month in the flood onset in some floodplain units, although the peak occurs in the same period of the river flood (May and June; *L6* and *L8*).

For the first time, our results show how the Amazon River floodplains are intensely active during the flood (May/June), with parallel riverine fluxes in floodplain units reaching from 2.5% to 20% of the main river discharge in the same period (*L9*) and water residence time ranging from 1.5 to 13 days (*L11*). This indicates that the Amazon floodplains work as a river, i.e., the Amazon River is the widest in the world during the flood considering the floodplain (20-50 km wide) as a continuous extension of the river. On the other hand, in the period of low connectivity with the river, the water residence time can be of several months and floodplain flows show negligible values relative to the flood period. The floodplain velocity fields are heterogeneous, with active flow channel and storage areas (*L10*). Furthermore, intense and weak floods promote, respectively, an increase and decrease of the period of high connectivity by 40 days due to the advance and delay of water inflow into the floodplain (*L12* and *L13*).

This study contributed to understanding of a dynamic and complex system. The 13 lessons learned about the Amazon floodplain hydrodynamics open a prospect to explore further questions, such as:

i) Evaluate and improve ratting-curves along the Amazon River, such as in Óbidos, since the floodplain fluxes is not currently considered.

ii) Understand the effects of intense floods, that have been more frequent in central Amazon (Chevuturi et al., 2022), on riparian communities.

iii) Improve the representation of hydrodynamic processes in floodplains in large-scale models (e.g. MGB and Camaflood).

iv) Understand nutrient and sediment variations in the floodplain, since the water mixing strongly influences the biogeochemical characteristics of the water (Wohl, 2021).

v) Estimate gas fluxes in the Amazon floodplain.

Acknowledgments

The authors would like to thank Conrado Rudorff and Walter Collischonn for their insights, and CNPq (Conselho Nacional de Desenvolvimento Científico e Tecnológico) for partially funding this research under the grant numbers 140352/2016-3 (A.C.F.A.). S.W. has been supported by the French AMANECER-MOPGA project funded by ANR and IRD (ref. ANR-18-MPGA-0008).

References

Abril, G., Martinez, J. M., Artigas, L. F., Moreira-Turcq, P., Benedetti, M. F., Vidal, L., et al. (2014). Amazon River carbon dioxide outgassing fuelled by wetlands. *Nature*, *505*(7483), 395–398. https://doi.org/10.1038/nature12797

Alsdorf, D., Rodriguez, E., & Lettenmaier, D. P. (2007). Measuring surface water from space. *Reviews of Geophysics*, *45*(2), 1–24. https://doi.org/10.1029/2006RG000197.1.INTRODUCTION

Alsdorf, D., Han, S. C., Bates, P., & Melack, J. (2010). Seasonal water storage on the Amazon floodplain measured from satellites. *Remote Sensing of Environment*, *114*(11), 2448–2456. https://doi.org/10.1016/j.rse.2010.05.020

Arcement Jr, G. J., & Schneider, V. R. (1989). Guide for Selecting Manning's Roughness Coefficients for Natural Channels and Flood Plains. *Technical Report, Geological Survey Water-Supply, United States Government Printing Office, Washington, U.S.A*, 38. https://doi.org/Report No. FHWA-TS-84-204

Armijos, E., Crave, A., Espinoza, J. C., Filizola, N., Espinoza-Villar, R., Ayes, I., et al. (2020). Rainfall control on amazon sediment flux: Synthesis from 20 years of monitoring. *Environmental Research Communications*, *2*(5). https://doi.org/10.1088/2515-7620/ab9003

Barbosa, C. C. F., Novo, E. M. L. de M., Melack, J. M., Freitas, R. M. de, & Pereira, W. (2006). A methodology for analysis of volume and flooded area dynamics: Lago Grande de Curuai várzea as an example. *Revista Brasileira de Cartografia*, *58*(3), 201–210.

Basso, L. S., Marani, L., Gatti, L. V., Miller, J. B., Gloor, M., Melack, J., et al. (2021). Amazon methane budget derived from multi-year airborne observations highlights regional variations in emissions. *Communications Earth & Environment*, *2*(1), 1–13. https://doi.org/10.1038/s43247-021-00314-4

Baugh, C. A., Bates, P. D., Schumann, G., & Trigg, M. A. (2013). SRTM vegetation removal and hydrodynamic modeling accuracy. *Water Resources Research*, *49*(9), 5276–5289. https://doi.org/10.1002/wrcr.20412

Beighley, R. E., Eggert, K. G., Dunne, T., He, Y., Gummadi, V., & Verdin, K. L. (2009). Simulating hydrologic and hydraulic processes throughout the Amazon River Basin. *Hydrological Processes*, *23*, 1221–1235. https://doi.org/10.1002/hyp

Birkett, C. M., Mertes, L. A. K., Dunne, T., Costa, M. H., & Jasinski, M. J. (2002). Surface water dynamics in the Amazon Basin: Application of satellite radar altimetry. *Journal of Geophysical Research D: Atmospheres*,

107(20). https://doi.org/10.1029/2001JD000609

Bonnet, M. P., Barroux, G., Martinez, J. M., Seyler, F., Moreira-Turcq, P., Cochonneau, G., et al. (2008). Floodplain hydrology in an Amazon floodplain lake (Lago Grande de Curuaí). *Journal of Hydrology*, *349*(1–2), 18–30. https://doi.org/10.1016/j.jhydrol.2007.10.055

Bonnet, M. P., Pinel, S., Garnier, J., Bois, J., Resende Boaventura, G., Seyler, P., & Motta Marques, D. (2017). Amazonian floodplain water balance based on modelling and analyses of hydrologic and electrical conductivity data. *Hydrological Processes*, *31*(9), 1702–1718. https://doi.org/10.1002/hyp.11138

Brunner, G. W. (2016). HEC-RAS river analysis system, User's Manual, Version 5.0. *US Army Corps of Engineers Hydrologic Engineering Center, Davis CA*, (February), 960.

Callède, J., Cochonneau, G., Alves, F. V., Guyot, J.-L., Guimarães, V. S., & De Oliveira, E. (2010). The River Amazon water contribution to the Atlantic Ocean. *Revue Des Sciences de l'eau*, *23*(3), 247–273. Retrieved from https://www.erudit.org/en/journals/rseau/2010-v23-n3-rseau3946/044688ar/abstract/

Cao, N., Lee, H., Jung, H. C., & Yu, H. (2018). Estimation of Water Level Changes of Large-Scale Amazon Wetlands Using ALOS2 ScanSAR Differential Interferometry, *10*(966). https://doi.org/10.3390/rs10060966

Chevuturi, A., Klingaman, N. P., Rudorff, C. M., Coelho, C. A. S., & Schöngart, J. (2022). Forecasting annual maximum water level for the Negro River at Manaus. *Climate Resilience and Sustainability*, *1*(1), 1–17. https://doi.org/10.1002/cli2.18

Chow, V. Te. (1959). Open-channel hydraulics. *McGraw-Hill Book Company*, 728. https://doi.org/ISBN 07-010776-9

Coe, M. T., Costa, M. H., & Howard, E. A. (2008). Simulating the surface waters of the Amazon River basin: Impacts of new river geomorphic and flow parameterizations. *Hydrological Processes*, *22*(14), 2542–2553. https://doi.org/10.1002/hyp.6850

Collischonn, W., Allasia, D., da Silva, B. C., & Tucci, C. E. M. (2007). The MGB-IPH model for large-scale rainfall-runoff modelling. *Hydrological Sciences Journal*, *52*(5), 878–895. https://doi.org/10.1623/hysj.52.5.878

Correa, S. W., Paiva, R. C. D. de, Espinoza, J. C., & Collischonn, W. (2017). Multi-decadal Hydrological Retrospective: Case study of Amazon floods and droughts. *Journal of Hydrology*, *549*, 667–684. https://doi.org/10.1016/j.jhydrol.2017.04.019

Dunne, T., Mertes, L. A. K., Meade, R. H., Richey, J. E., & Forsberg, B. R. (1998). Exchanges of sediment between the flood plain and chennel of the Amazon River in Brazil. *Geological Society of America Bulletin*, *110*(December 1997), 450–467. https://doi.org/10.1130/0016-7606(1998)110<0450

Duponchelle, F., Isaac, V. J., Rodrigues Da Costa Doria, C., Van Damme, P. A., Herrera-R, G. A., Anderson, E. P., et al. (2021). Conservation of migratory fishes in the Amazon basin. *Aquatic Conservation: Marine and Freshwater Ecosystems*, *31*(5), 1087–1105. https://doi.org/10.1002/aqc.3550

Fassoni-Andrade, A. C., Paiva, R. C. D., Rudorff, C. M., Barbosa, C. C. F., & Novo, E. M. L. de M. (2020a). High-resolution mapping of floodplain topography from space: A case study in the Amazon. *Remote Sensing of Environment*, *251*, 112065. https://doi.org/10.1016/j.rse.2020.112065

Fassoni-Andrade, A. C., Fleischmann, A. S., Paiva, R. C. D. (2020b). Lake topography and active storage from satellite observations of flood frequency. *Water Resources Research*, 56(7). https://doi.org/10.1029/2019wr026362

Fassoni-Andrade, A. C., Fleischmann, A. S., Papa, F., Paiva, R. C. D. de, Wongchuig, S., Melack, J. M., et al. (2021). Amazon Hydrology From Space: Scientific Advances and Future Challenges. *Reviews of Geophysics*, *59*(4), 1–97. https://doi.org/10.1029/2020RG000728

Ferreira-Ferreira, J., Silva, T. S. F., Streher, A. S., Affonso, A. G., De Almeida Furtado, L. F., Forsberg, B. R., et al. (2014). Combining ALOS/PALSAR derived vegetation structure and inundation patterns to characterize major vegetation types in the Mamirauá Sustainable Development Reserve, Central Amazon floodplain, Brazil. *Wetlands Ecology and Management*, *23*(1), 41–59. https://doi.org/10.1007/s11273-014-9359-1

Filizola, N., Latrubesse, E. M., Fraizy, P., Souza, R., Guimarães, V., & Guyot, J. L. (2014). Was the 2009 flood the most hazardous or the largest ever recorded in the Amazon? *Geomorphology*, *215*, 99–105. https://doi.org/10.1016/j.geomorph.2013.05.028

Fleischmann, A. S., Paiva, R. C. D., Collischonn, W., Sorribas, M. V., & Pontes, P. R. M. (2016). On river-floodplain interaction and hydrograph skewness. *Water Resources Research*, *52*(10), 7615–7630. https://doi.org/10.1002/2016WR019233

Fleischmann, A. S., Paiva, R., & Collischonn, W. (2019). Can regional to continental river hydrodynamic models be locally relevant? A cross-scale comparison. *Journal of Hydrology X*, *3*, 100027. https://doi.org/10.1016/j.hydroa.2019.100027

Fleischmann, A. S., Papa, F., Fassoni-Andrade, A., Melack, J. M., Wongchuig, S., Paiva, R. C. D. de, et al. (2022). How much inundation occurs in the Amazon River basin? *Remote Sensing of Environment*, *278*(June), 67. https://doi.org/10.1002/essoar.10508718.1

Frappart, F., Papa, F., Güntner, A., Tomasella, J., Pfeffer, J., Ramillien, G., et al. (2019). The spatio-temporal variability of groundwater storage in the Amazon River Basin. *Advances in Water Resources*, *124*(October 2016), 41–52. https://doi.org/10.1016/j.advwatres.2018.12.005

Fricke, A. T., Nittrouer, C. A., Ogston, A. S., Nowacki, D. J., Asp, N. E., & Souza Filho, P. W. M. (2019). Morphology and dynamics of the intertidal floodplain along the Amazon tidal river. *Earth Surface Processes and Landforms*, *44*(1), 204–218. https://doi.org/10.1002/esp.4545

Getirana, A. C. V., Boone, A., Yamazaki, D., Decharme, B., Papa, F., & Mognard, N. (2012). The Hydrological Modeling and Analysis Platform (HyMAP): Evaluation in the Amazon Basin. *Journal of Hydrometeorology*, *13*(6), 1641–1665. https://doi.org/10.1175/JHM-D-12-021.1

Hess, L. L., Melack, J. M., Novo, E. M. L. M. L. M., Barbosa, C. C. F. F., & Gastil, M. (2003). Dual-season mapping of wetland inundation and vegetation for the central Amazon basin. *Remote Sensing of Environment*, *87*(4), 404–428. https://doi.org/10.1016/j.rse.2003.04.001

Hess, L. L., Melack, J. M., Affonso, A. G., Barbosa, C., Gastil-Buhl, M., & Novo, E. M. L. M. (2015). Wetlands of the Lowland Amazon Basin: Extent, Vegetative Cover, and Dual-season Inundated Area as Mapped with JERS-1 Synthetic Aperture Radar. *Wetlands*, *35*(4), 745–756. https://doi.org/10.1007/s13157-015-0666-y

Ji, X., Lesack, L. F. W., Melack, J. M., Wang, S., Riley, W. J., & Shen, C. (2019). Seasonal and inter-annual patterns and controls of hydrological fluxes in an Amazon floodplain lake with a surface-subsurface processes model. *Water Resources Research*, *55*(4), 3056–3075. https://doi.org/10.1029/2018WR023897

Latrubesse, E. M., & Franzinelli, E. (2002). The Holocene alluvial plain of the middle Amazon River, Brazil. *Geomorphology*, *44*(3–4), 241–257. https://doi.org/10.1016/S0169-555X(01)00177-5

LeFavour, G., & Alsdorf, D. (2005). Water slope and discharge in the Amazon River estimated using the shuttle radar topography mission digital elevation model. *Geophysical Research Letters*, *32*(17), 1–5. https://doi.org/10.1029/2005GL023836

Lesack, F. W., & Melack, J. M. (1995). Flooding hydrology and mixture dynamics of lakewater derived from multiple sources in an Amazon floodplain lake. *Water Resources Research*, *31*(2), 329–345.

Luo, X., Li, H. Y., Ruby Leung, L., Tesfa, T. K., Getirana, A., Papa, F., & Hess, L. L. (2017). Modeling surface water dynamics in the Amazon Basin using MOSART-Inundation v1.0: Impacts of geomorphological parameters and river flow representation. *Geoscientific Model Development*, *10*(3), 1233–1259. https://doi.org/10.5194/gmd-10-1233-2017

Melack, J. M., Novo, E. M. L. M., Forsberg, B. R., Piedade, M. T. F. F., & Maurice, L. (2009). Floodplain Ecosystem Processes. *Amazonia and Global Change*, (2003), 525–541. https://doi.org/10.1029/2008GM000727

Paiva, R. C. D. de, Buarque, D. C., Collischonn, W., Bonnet, M. P., Frappart, F., Calmant, S., & Bulhões Mendes, C. A. (2013). Large-scale hydrologic and hydrodynamic modeling of the Amazon River basin. *Water Resources Research*, *49*(3), 1226–1243. https://doi.org/10.1002/wrcr.20067

Papa, F., Frappart, F., Güntner, A., Prigent, C., Aires, F., Getirana, A. C. V, & Maurer, R. (2013). Surface freshwater storage and variability in the Amazon basin from multi-satellite observations, 1993-2007. *Journal of Geophysical Research Atmospheres*, *118*(21), 11951–11965. https://doi.org/10.1002/2013JD020500

Pinel, S., Bonnet, M.-P., Santos Da Silva, J., Moreira, D., Calmant, S., Satgé, F., & Seyler, F. (2015). Correction of Interferometric and Vegetation Biases in the SRTMGL1 Spaceborne DEM with Hydrological Conditioning towards Improved Hydrodynamics Modeling in the Amazon Basin. *Remote Sensing*, *7*(12), 16108–16130. https://doi.org/10.3390/rs71215822

Pinel, S., Bonnet, M., Silva, J. S. Da, Sampaio, T. C., Garnier, J., Catry, T., et al. (2019). Flooding dynamics within a Amazonian floodplain : Water circulation patterns and inundation duration. *Water Resources Research*, *56*(1). https://doi.org/10.1029/2019WR026081

Richey, J. E., Mertes, L. K., Dunne, T., Victoria, R. L., Forsberg, B. R., Tancredi, A. C. N. S., & Oliveira, E. de. (1989). Sources and routing of the Amazon River flood wave, *3*(3), 191–204.

Rosenqvist, J., Rosenqvist, A., Jensen, K., & McDonald, K. (2020). Mapping of maximum and minimum inundation extents in the amazon basin 2014-2017 with ALOS-2 PALSAR-2 scan SAR time-series data. *Remote Sensing*, *12*(8). https://doi.org/10.3390/RS12081326

Rudorff, C. M., Melack, J. M., & Bates, P. D. (2014a). Flooding dynamics on the lower Amazon floodplain: 1. Hydraulic controls on water elevation, inundation extent, and river-floodplain discharge. *Water Resources Research*, *50*(1), 619–634. https://doi.org/10.1002/2013WR014091

Rudorff, C. M., Melack, J. M., & Bates, P. D. (2014b). Flooding dynamics on the lower Amazon floodplain: 2. Seasonal and interannual hydrological variability. *Water Resources Research*, *50*(1), 635–649. https://doi.org/10.1002/2013WR014714

Schumann, G., Bates, P. D., Horritt, M. S., Matgen, P., & Pappenberger, F. (2009). Progress in Integration of Remote Sensing-Derived Flood Extent and Stage Data and Hydraulic Models. *Reviews of Geophysics*, *47*(2008), 1–20. https://doi.org/10.1029/2008rg000274

Silva, J. S. Da, Calmant, S., Seyler, F., Rotunno Filho, O. C., Cochonneau, G., & Mansur, W. J. (2010). Water levels in the Amazon basin derived from the ERS 2 and ENVISAT radar altimetry missions. *Remote Sensing of Environment*, *114*(10), 2160–2181. https://doi.org/10.1016/j.rse.2010.04.020

Siqueira, V. A., Paiva, R. C. D., Fleischmann, A. S., Fan, F. M., Ruhoff, A. L., Pontes, P. R. M., et al. (2018). Toward continental hydrologic-hydrodynamic modeling in South America. *Hydrology and Earth System Sciences*, *22*(9), 4815–4842. https://doi.org/10.5194/hess-22-4815-2018

Sorribas, M. V., de Paiva, R. C. D., Fleischmann, A. S., & Collischonn, W. (2020). Hydrological Tracking Model for Amazon Surface Waters. *Water Resources Research*, *56*(9), 1–19. https://doi.org/10.1029/2019WR024721

Trigg, M. A., Wilson, M. D., Bates, P. D., Horritt, M. S., Alsdorf, D. E., Forsberg, B. R., & Vega, M. C. (2009). Amazon flood wave hydraulics. *Journal of Hydrology*, *374*(1–2), 92–105. https://doi.org/10.1016/j.jhydrol.2009.06.004

Trigg, M. A., Bates, P. D., Wilson, M. D., Schumann, G., & Baugh, C. (2012). Floodplain channel morphology and networks of the middle Amazon River. *Water Resources Research*, *48*(10), 1–17. https://doi.org/10.1029/2012WR011888

Tull, N., Passalacqua, P., Hassenruck-Gudipati, H. J., Rahman, S., Wright, K., Hariharan, J., & Mohrig, D. (2022). Floodplain Connectivity During Combined Pluvial-Fluvial Events. *Water Resources Research*, *58*(3), 1–24. https://doi.org/10.1029/2021WR030492

Wilson, M. D., Bates, P., Alsdorf, D., Forsberg, B., Horritt, M., Melack, J., et al. (2007). Modeling large-scale inundation of Amazonian seasonally flooded wetlands. *Geophysical Research Letters*, *34*(15), 4–9. https://doi.org/10.1029/2007GL030156

Wohl, E. (2021). An Integrative Conceptualization of Floodplain Storage. *Reviews of Geophysics*, *59*(2), 1–63. https://doi.org/10.1029/2020RG000724

Yamazaki, D., Kanae, S., Kim, H., & Oki, T. (2011). A physically based description of floodplain inundation dynamics in a global river routing model. *Water Resources Research*, *47*(4). https://doi.org/10.1029/2010WR009726

Yamazaki, D., Baugh, C. A., Bates, P. D., Kanae, S., Alsdorf, D. E., & Oki, T. (2012). Adjustment of a spaceborne DEM for use in floodplain hydrodynamic modeling. *Journal of Hydrology*, *436–437*, 81–91. https://doi.org/10.1016/j.jhydrol.2012.02.045

Yamazaki, D., Lee, H., Alsdorf, D. E., Dutra, E., Kim, H., Kanae, S., & Oki, T. (2012). Analysis of the water level dynamics simulated by a global river model: A case study in the Amazon River. *Water Resources Research*, *48*(9), 1–15. https://doi.org/10.1029/2012WR011869

Yamazaki, D., Ikeshima, D., Tawatari, R., Yamaguchi, T., O'Loughlin, F., Neal, J. C., et al. (2017). A high-accuracy map of global terrain elevations. *Geophysical Research Letters*, *44*(11), 5844–5853. https://doi.org/10.1002/2017GL072874

Zhang, Q., & Werner, A. D. (2015). Hysteretic relationships in inundation dynamics for a large lake-floodplain system. *Journal of Hydrology*, *527*, 160–171. https://doi.org/10.1016/j.jhydrol.2015.04.068